Current Research in Food Science 5 (2022) 2251–2260

Contents lists available at ScienceDirect

Current Research in Food Science

journal homepage: www.sciencedirect.com/journal/current-research-in-food-science

Bioactivity guided isolation and identification of phenolic compounds from *Citrus aurantium* L. with anti-colorectal cancer cells activity by UHPLC-Q-TOF/MS

Li Gao [a], Na Gou [a], William Kwame Amakye [a], Jianlin Wu [b], Jiaoyan Ren [a,*]

[a] School of Food Science and Engineering, South China University of Technology, Guangzhou, Guangdong, China
[b] State Key Laboratory for Quality Research in Chinese Medicines, Macau University of Science and Technology, Macau, China

ARTICLE INFO

Keywords:
Bioactivity guided isolation
Citrus aurantium L.
Phenolic compounds
Colorectal cancer
Wnt signalling

ABSTRACT

Natural plants are rich sources of various bioactive compounds. Consequently, the efficiently isolation of these bioactive components has always attracted considerable attention. Our work aims to demonstrate a framework for bioactivity guided isolation of potential effective compounds from the complex food materials. We demonstrated its application for isolation of phenolic compounds with anti-proliferative activity against colorectal cancer cells (CRCs) from *Citrus aurantium* L. Firstly, phenolic rich fraction was successfully identified as the main effective components that could simultaneously suppress the growth of CRCs and inhibit Wnt signaling. In order to obtain the bioactive phenolic constituents, a detailed study was performed by optimizing the purification conditions. Two phenolic rich fractions (40% and 60% ethanol elution fractions) were then obtained by AB-8 macroporous resins under optimized condition. Finally, the main components (65 compounds) were tentatively identified from the 40% ethanol eluant by ultra-high performance liquid chromatography-quadrupole time-of-flight mass spectrometry (UHPLC-Q-TOF/MS) analysis. Notably, there were five of the phytochemicals (Feruloylagmatine, Haploside C, Sagittatin A, Linderagalactone C and Koparin-2′-methyl ether) which were hitherto unidentified in *Citrus aurantium* L. fruit. In conclusion, this study showed that under the principle of bioactivity guided strategy, phenolic constituents with potential anti-CRCs activity were isolated from *Citrus aurantium* L.

1. Introduction

Natural plants are rich sources of various bioactive compounds as such they are attracting significant attention in the functional food and pharmaceutical industries owing to their irreplaceable advantages, such as safety, convenience in accessibility and higher acceptability for long-term intake (Gao et al., 2021). However, efficient isolation and analysis of the bioactive compounds from plant food still remain a huge challenge. Usually, phytochemicals isolation is guided according to the principle of yield maximization without functional evaluation during the isolation process. It may lead to the loss of some effective components under inappropriate conditions. In addition, it may not be the most efficient way to isolate bioactivity components from complex materials. To address this issue, the concept of bioactivity-guided isolation was proposed and has become an attractive approach for bioactive molecular profiling and screening (Chen et al., 2015; Pezzuto, 1997).

Citrus aurantium L., as a rich source of phenolic compounds especially hesperidin, naringin and nobiletin (Khan et al., 2014; Singh et al., 2020), is a common citrus fruit with numerous demonstrable benefits for intestinal health (Degirmenci and Erkurt, 2020; Farahmandfar et al., 2020; Shehata et al., 2021). Numerous studies have indicated the excellent capabilities of citrus bioactive compounds in regulating cellular homeostasis in CRC and their chemopreventive properties against CRCs (Jayaprakasha et al., 2008; Odeh et al., 2021; Patil et al., 2009). However, for the anti- CRCs effects of *Citrus aurantium* L., most studies have mainly focused on the essential oil of its flowers or leaves

Abbreviations: **CRCs**, colorectal cancer cells; **DMEM**, dulbecco's modified Eagle's medium; **FBS**, fetal bovine serum; **PBS**, phosphate-buffered saline; **MTT**, 3-; 4, 5-dimethyl-2-thiazolyl, -2, 5-diphenyl-2-H-tetrazolium bromide; **TPC**, total phenolic content; **BV**, bed volume; **UHPLC-Q-TOF/MS**, ultra-high performance liquid chromatography-quadrupole time-of-flight mass spectrometry; **CM**, conditioned medium; **TIC**, total ion current.

* Corresponding author.
E-mail address: jyren@scut.edu.cn (J. Ren).

https://doi.org/10.1016/j.crfs.2022.11.013
Received 31 March 2022; Received in revised form 19 October 2022; Accepted 12 November 2022
Available online 17 November 2022

(Almalki, 2021; Majnooni et al., 2012; Odeh et al., 2021). Less attention has paid to the *Citrus aurantium* L. fruits, which is rich in phenolic compounds. Therefore, there is a great potential to explore the effective phenolic compounds in *Citrus aurantium* L. fruits, as promising future functional food ingredients for CRC chemopreventive.

In this study, CRCs with high proliferation characteristics were chosen as *in vitro* screening model to isolate active phenolic components from *Citrus aurantium* L. by bioactivity-guided rule. In CRC, hyperactivation of the Wnt signaling is suggested to be the key oncogenic driver, and thus has been considered as a therapeutic target to screen small molecular agents for CRC intervention (Li et al., 2022; Song et al., 2015). Therefore, the inhibitory effects on the Wnt signaling and the proliferation of CRCs are regarded as the main indicators for the screening of bioactive food components.

We described a bioactivity-guided isolation method via anti-CRCs profiling based on UHPLC-Q-TOF/MS to identify effective components from *Citrus aurantium* L.. During the whole isolation process, we mainly evaluated the activity of each fraction by EdU (5-ethynyl-2′-deoxyuridine) assay and dual-luciferase reporter assay system. We first focused on identifying the main category of compounds with anti-CRC activity. Subsequently, a detailed study was conducted by optimizing the purification conditions. Two phenolic rich fractions were then purified using AB-8 resins under optimized conditions. Finally, the effects of the purified fractions on the proliferation of Wnt-dependent CRCs were evaluated and their constituents were characterized by UHPLC-Q-TOF/MS analysis.

2. Materials and methods

2.1. Materials

RKO and HCT116 cells, HEK293 reporters, Wnt3a-secreting L cells were generous gifts from professor Jieqiong Tan. Dulbecco's modified Eagle's medium (DMEM), fetal bovine serum (FBS) and phosphate-buffered saline (PBS, pH 7.4) were purchased from Thermo Fisher Scientific (Waltham, MA, USA). Folin-Ciocalteu reagent and 3-(4, 5-dimethyl-2-thiazolyl)-2, 5-diphenyl-2-H-tetrazolium bromide (MTT) and were purchased from Sigma-Aldrich (St. Louis, MO, USA). *Citrus aurantium* L. were purchased from YiFang Chinese traditional medicine (Guangdong, China). NKA-9, ADS-17, AB-8 and D101 macroporous resins were obtained from Cangzhou Bon Adsorber Technology Co. Ltd (Tianjin, China).

2.2. The extraction of Citrus aurantium L

The dried *Citrus aurantium* L. decoction pieces were powdered by a laboratory mill and passed through a 60-mesh screen. *Citrus aurantium* L. powder was extracted with water and ethanol (75% v/v) at the ratio of 1:10, respectively, at a temperature of 60°C for 60 min with ultrasonic assistance (45 kHz). The solution was then centrifuged for 10 min at a speed of 10000 rpm. The supernatant was acquired and concentrated in a rotary evaporator at 50°C to obtain the crude extracts. The crude extracts were frozen at -20°C and then they are freeze-dried by freeze dryer.

2.3. Total phenolic content (TPC)

TPC of the extracts was measured by the Folin-Ciocalteu method with minimal adjustments. Briefly, a 1 mL sample or standard solution was mixed with 2.5 mL of Folin–Ciocalteu reagent (1:1 v/v), 2.5 mL of saturated Na_2CO_3 (7.5% w/v) and 4 mL deionized water and then kept at room temperature for 1 h. The absorbance was measured at 756 nm using an ultraviolet–visible absorbance spectrophotometer (Synergy H1, BioTek). A calibration curve for the gallic acid standards (at concentrations of 0.01, 0.02, 0.03, 0.04, 0.05 and 0.06 mg/mL) was done. The linear regression equation was $y = 0.008933x + 0.009525$ and $R^2 = 0.9986$. The TPC was expressed as μg gallic acid equivalent (μg GAE/mL).

2.4. Static adsorption and desorption properties of macroporous resins

The resins were pretreated according to the previous method with minimal modifications (Ren et al., 2017). First, the resins were first soaked with four times 95% (v/v) ethanol for 24 h and then washed with distilled water. They were immersed in 0.5 mol/L HCl and 0.5 mol/L NaOH solution 3 times in turn and each time for 4 h. Next, they were fully washed in distilled water until the water flowing out is neutral (pH = 7.0). Ultimately, four resins were dried at 60°C in a drying oven (DHG-070, Shanghai Yiheng Thermostatic Equipment Co. Ltd, Shanghai, China) to reach constant weight.

Four aliquots (2.00 g dry basis) of each resin were separately added into four 150 mL flasks. First, the resins were activated with 100 mL 95% (v/v) ethanol for 10 h, and then the ethanol was washed with deionized water thoroughly. Each resin in flask were soaked in 20 mL crude extracts at 10 mg/mL. Then the flasks were shaken by using a shaking incubator with a speed of 200 rpm at room temperature for 12 h. After adsorption equilibrium, the resins were washed with distilled water. Then, 20 mL of 95% (v/v) ethanol was poured into the flasks for desorption. The flasks were shaken as same as the adsorption process. After both adsorption and desorption equilibrium, the solutions were filtered, and the adsorption and desorption ratios of each resin were calculated using the following equations:

$$\text{Adsorption capacity}: \ Q_e\ (\text{mg GAE}/\text{g}) = \frac{(C_0 - C_e) \times V_o}{m} \quad (1)$$

$$\text{Desorption capacity}: \ D\ (\text{mg GAE}/\text{g}) = \frac{C_d \times V_d}{m} \quad (2)$$

$$\text{Desorption ratio}: \ R(\%) = \frac{C_d \times V_d}{(C_0 - Ce) \times V_0} \times 100\% \quad (3)$$

m: the weight of the macroporous resins (g).

C_0: the initial concentration of TPC in solution (mg GAE/mL).

C_e: the equilibrium concentration of TPC in solution (mg GAE/mL).

C_d: the equilibrium concentration of TPC in desorption solution (mg GAE/mL).

V_0: the volume of the initial extract solution (mL).

V_d: the volume of the desorption solution (mL).

2.5. Adsorption and desorption kinetics

1.00 g (dry basis) of the pretreated AB-8 resins and 10.00 mL of ethanol extracts (1400.00 μg GAE/mL) were added into a flask. The flask was sealed and shaken on an oscillator at 200 rpm for 24 h at 25°C. After adsorption, the resins were washed five times with distilled water. Next, 10.00 mL 95% (v/v) ethanol and the resins were put into another flask and shaken at 200 rpm for 24 h at 25°C.

2.6. Adsorption isotherms

Ethanol extracts with TPCs of 0.22, 0.43, 0.86, 1.72, 3.44, 6.88 mg GAE/mL were prepared. 10.00 mL of each solution and 1.00 g (dry basis) AB-8 resins were added into the flask at 25°C, 35°C and 45°C, respectively. The following process was performed as described in the section 2.4.

2.7. Dynamic adsorption and desorption with AB-8 macroporous resins

The dynamic adsorption and desorption experiments were performed on a glass column (2.60 cm × 40.00 cm) with pre-treated AB-8 resins. The bed volume (BV) of the AB-8 resins was 100 mL. Briefly, 100 mL of the crude extracts (1.00 mg GAE/mL) was added onto the top of

the column and hold at room temperature (25°C) for 2.5 h to reach adsorption equilibrium. After adsorption, the resins were washed with 3BV distilled water and then eluted with different concentrations of ethanol (10%, 20%, 40%, 60% and 80%, v/v). The flow rate was 1.5 mL/min and the elution volume of each ethanol solution was 4BV. Eluents were collected at 7 mL/tube by an auto-fraction collector and TPCs of the eluents were examined every two tubes by Folin–Ciocalteu method. The collected two fractions, fraction 1 (eluted with 40% ethanol) and fraction 2 (eluted with 60% ethanol), were concentrated in a rotary evaporator at 50°C and stored at 20°C for further analysis.

2.8. UHPLC-Q-TOF/MS analysis

We used an Agilent 1290 Infinity LC system (UHPLC, Santa Clara, CA) that consisted of an auto sampler, thermostatic column compartment, and binary pump with an Agilent Eclipse plus-C18 column (2.1 × 100 mm, 1.8 μm). The auto sampler was set at 4°C and the column temperature was maintained at 30°C. The mobile phases were A: 0.1% formic acid in water and B: 0.1% formic acid in acetonitrile. Two solvents were eluted at a flow rate of 0.3 mL/min according to the following gradient: 0–0.5 min, 2% B; 0.5–2.5 min, 2%–6% B; 2.5–12.0 min, 6%–15% B; 12.0–22.0 min, 15%–25% B; 22.0–27.0 min, 25%–30% B; 27.0–45.0 min, 30%–55% B; 45.0–47.0 min, 55%–95% B; 47.0–49.5 min, 95% B; 50.0 min, 2% B, and kept for 3 min as a rebalance step. The injection volume in the UHPLC system was 1 μL. HRMS analyses were performed on an Agilent 6545 UHD accurate-mass Q-TOF/MS system with dual jet stream electrospray ion source (dual AJS ESI) using positive (POS) ion mode. The MS parameters were set as follows: dry gas temperature is 300°C, dry gas flow at 15 L/min, sheath gas temperature is 325 °C, sheath gas flow at 11 L/min, nebulizer pressure is 35 psig, capillary voltage is 4500 V, and nozzle voltage is 500 V. The mass spectra of samples were recorded in the range of 150–1200 m/z. Accurate mass measurements were by using a low flow of TOF reference mixture, including the internal reference masses at m/z 122.0509 (C5H4N4) and m/z 922.0098 (C18H18F24N3O6P3) for POS ion mode. Moreover, ramped collision energy values for automatic MS/MS experiments were performed as follows: charge 1; slope 3; offset 15 eV. Using Nitrogen as drying, nebulizing and collision gas. MS data acquisition was processed using MassHunter Qualitative Analysis software (Agilent Technologies, USA). Identify the compounds based on retention time, elemental composition, and product ion spectrum to those in the literature and searching mass spectrometry information in METLIN (https://metlin.scripps.EdU/index.php) and MoNA (https://mona.fiehnlab.ucdavis.EdU/).

2.9. Cells and cell culture

RKO, HCT116 and HEK 293 cells were cultured in DMEM containing 10% (v/v) heat-inactivated FBS and 1% (v/v) streptomycin - penicillin solution. Cells were cultured in humidified atmosphere containing 95%

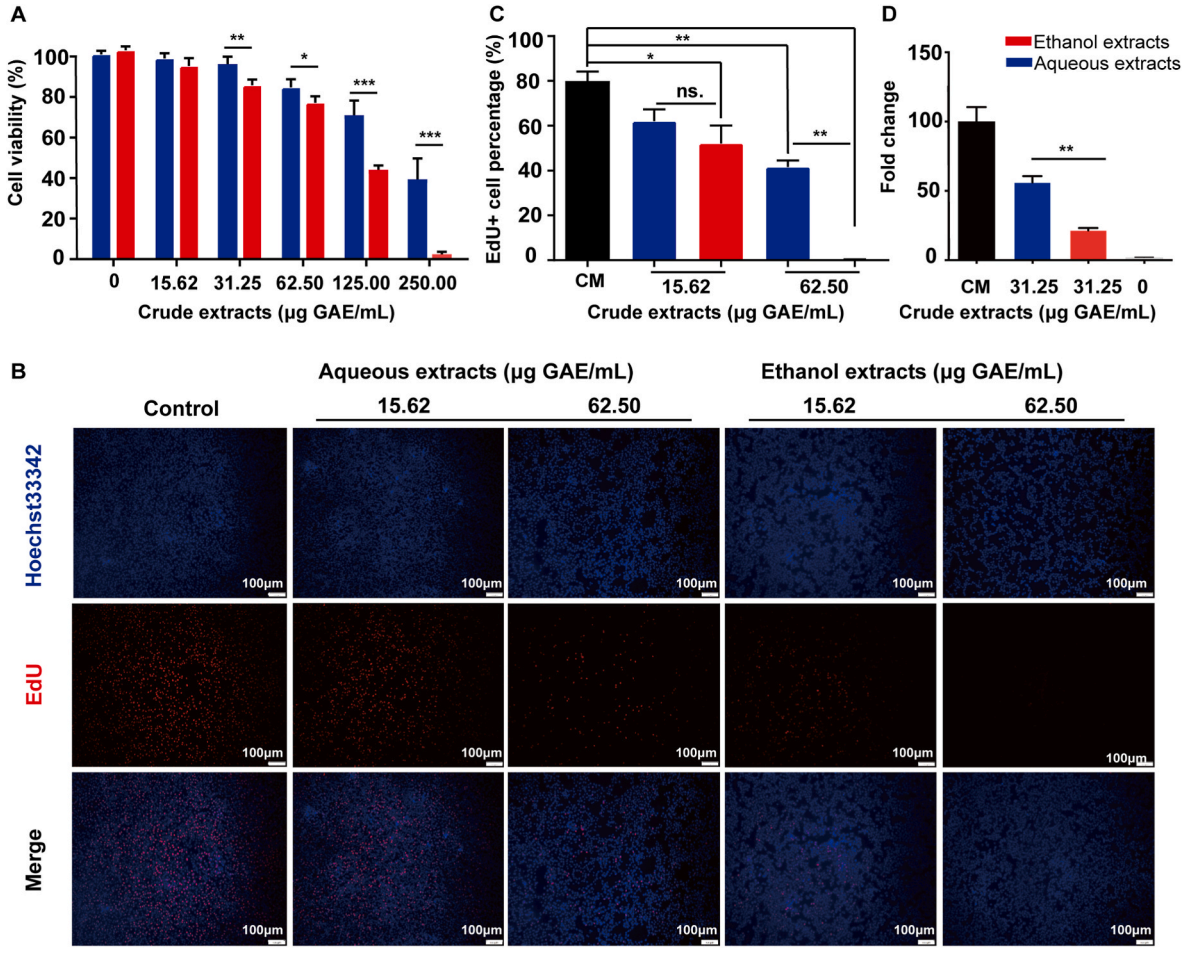

Fig. 1. Ethanol extracts from *Citrus aurantium* L. showed stronger capacities to inhibit the proliferation of RKO cells and the Wnt signaling than that of the aqueous extracts. A. MTT assay for aqueous and ethanol extracts in RKO cells. B. EdU assay for aqueous and ethanol extracts in RKO cells. Red fluorescence represents the EdU-incorporating cells (proliferation-positive cells), and blue fluorescence represents the cell nucleus. C. Quantification of EdU^+ cells by image J software. D. Dual-luciferase reporter assay for aqueous and ethanol extracts. $^*p < 0.05$, $^{**}p < 0.01$, $^{***}p < 0.001$. (Student's two tailed *t*-test). (For interpretation of the references to color in this figure legend, the reader is referred to the Web version of this article.)

O_2/5% CO_2 at 37°C.

2.10. MTT assay

Cells were seeded at a density of 2×10^4 per well in a 96-well plate for 16 h. Cells were then treated with samples (water and ethanol extracts, different fractions) at 37°C for another 24 h. MTT solution (5.0 mg/mL) was then added and further incubated at 37 °C for 4 h. Next, the medium was removed and 150 μL dimethyl sulfoxide was added into each well to dissolve the formazan crystals and incubated at 37°C for 10 min. Measure the absorbance at 570 nm by a BioTek SynergyH1 microplate reader (BioTek, USA). All experiments were done three times with triplicate.

2.11. Luciferase activity assay

Dual-luciferase gene assay is a sophisticated approach to evaluate the transduction activity of the Wnt/β-catenin signaling pathway. The TCF/β-catenin complex is a downstream transcriptional factor in the Wnt pathway. HEK293 reporters have been stably co-transfected with TOP-flash/FOP-flash plasmids containing wild-type and mutated TCF-binding site, respectively. A FOP-flash luciferase reporter was used as an internal control. Thus, increased/decreased TOP-flash reporter activity can indicate activation/inhibition status of the Wnt signaling.

HEK293 reporters were seeded in 96-well plates at a density of 2.0×10^4 cells/well and incubated in 95% O_2/5% CO_2 at 37°C for 16 h. The cells were incubated with different samples (water and ethanol extracts, different fractions) separately (each sample was dissolved in Wnt 3a conditioned medium (CM)) for 24 h. The luciferase activity was determined using the dual Luciferase Reporter Gene Assay Kit (Promega, Madison, USA) following manufacturer's instructions using BioTek SynergyH1 micro-plate reader. The result was calculated as fold change. All assays were performed in triplicate and repeated for three times. The result was expressed as TOP-flash activity normalized to FOP-flash activity.

Fold change = Fluorescence of TOP-flash (Firefly Luciferase)/Fluorescence of FOP-flash (Renilla Luciferase).

Wnt3a CM was used to stimulate the Wnt signaling, therefore to determine the inhibitory activity of the samples. For the Wnt3a CM preparation, Wnt3a-secreting L cells were cultured in 10 mL DMEM with 10% FBS for 4 d. Then the medium was harvested and sterilized by a 0.22 μm sterile filter. 10 mL fresh medium was added, and the cells were cultured for another 3 days, finally the medium were collected and mixed with the previous medium in the ratio of 1:1 and stored at −20°C.

2.12. EdU incorporation assay

Cells were seeded at a density of 2×10^4 per well in a 96-well plate for 16 h. Cells were then treated with samples (water and ethanol extracts, different fractions) at 37°C for another 24 h. Next, cells were treated with EdU (20 μM, dissolved in medium) and incubated for 2 h and then fixed with 4% paraformaldehyde for 15 min. Next, cells were permeabilized with 0.5% Triton X-100 at 25°C for 20 min. The EdU staining was followed with the BeyoClick™ EdU-555 Kit (Beyotime, Shanghai, China) and viewed with an inverted fluorescent microscope (Olympus, Tokyo, Japan). Six random fields of vision were captured in each group. Proliferation rate refers to the ratio of the number of EdU stained cells to the number of Hoechst 33342 stained cells. All assays were done three times with triplicate.

2.13. Statistical analysis

Data was presented as mean ± SD. Differences between group means were analyzed using student's two tailed *t*-test by SPSS software (version 24.0). GraphPad Prism software (Version 8.3) was used for graphical representation. Differences were deemed statistically significant when $p < 0.05$.

3. Results and discussion

3.1. Citrus aurantium L. extracts differential inhibited the proliferation of CRCs and the Wnt signaling

In order to select the *Citrus aurantium* L. extracts with higher anti-CRCs activity, the bioactivity of the aqueous extracts and ethanol extracts were compared. MTT assay results indicated that ethanol extracts from *Citrus aurantium* L. showed obvious stronger inhibitory activity on the growth of RKO CRCs within the concentration range of 31.25–250.00 μg GAE/mL (Fig. 1A). Briefly, both showed dose-dependent inhibitory effect. The crude ethanol extracts significantly reduced the viability of RKO cells to 2.46 ± 1.19% at the concentration of 250.00 μg GAE/mL ($p < 0.001$), indicating that the ethanol extracts preferentially inhibited CRCs growth. To further confirm the anti-proliferative activity of ethanol extracts on CRCs, EdU incorporation assay was performed to detect DNA synthesis on proliferating CRCs. The newly synthesized DNA was labelled by the alkyne group of EdU, which enabled the proliferating cells to be detected with fluorescent microscopy. The EdU assay revealed that both extracts dose-dependently inhibited RKO cells proliferation (Fig. 1 B, C). At the concentration of 62.50 μg GAE/mL, the proliferation rate of RKO was reduced to 41.59 ± 2.91% by the treatment of aqueous extracts, while ethanol extracts almost completely inhibited the proliferation of RKO cells. The results further demonstrated that the ethanol extracts possessed stronger anti-CRC activity.

Wnt signaling is an evolutionarily conserved pathway that regulates the proliferation of cells (Nusse and Clevers, 2017). In CRC, aberrant activated Wnt signaling is one of the major causes of CRCs proliferation. To further determine the anti-CRC behaviour of aqueous and ethanol extracts at the molecular level, their regulatory effects on Wnt signaling were evaluated. The highly sensitive dual-luciferase reporter system was applied to identify the potential effects on the Wnt signaling pathway. Ethanol extracts showed stronger inhibitory effect (21.59 ± 1.63%) on the Wnt signaling compared with aqueous extracts (56.15 ± 4.58%) at 62.50 μg GAE/mL (Fig. 1D).

Taken together, these results suggested that more active components with anti-CRCs and potential Wnt inhibitory activity exist in ethanol extracts, in which the observed differences in anti-CRC activities were affected by the applied extracting solvent. Since extraction solvents could affect the variety and proportion of the constituents, for instance, higher yield of polyphenol from Beijing propolis can be obtained in 75% ethanol/water solvent compared with water and different ethanol/water solvents (C. Sun et al., 2015). Results of previous works have also demonstrated that the bioactivity of plant extracts depends largely on the extraction solvent (Sarikurkcu et al., 2019).

3.2. Citrus aurantium L. polyphenols are the effective components

Plant polyphenols are always considered as promising bioactive compounds for their various cancer preventive effects (Niedzwiecki et al., 2016). The stronger bioactivity of the ethanol extracts may be due to the higher polyphenol contents, since polyphenols are more easily extracted by ethanol solvent. We proposed that the *Citrus aurantium* L. polyphenols are the main effective components with anti-CRCs activity by attenuating Wnt signaling. In this regard, we designed a simple experiment to verify the hypothesis.

Generally, crude *Citrus aurantium* L. extracts contain multiple ingredients besides polyphenols. In such a complex substance system, it is difficult to distinguish of the components responsible for the inhibition of the proliferation of CRCs. In this regard, AB-8 macroporous resin was applied for the preliminary separation of phenolic compounds to determine if the phenolic rich fraction is the main target constituents. The ethanol extracts were treated by AB-8 macroporous resins using the

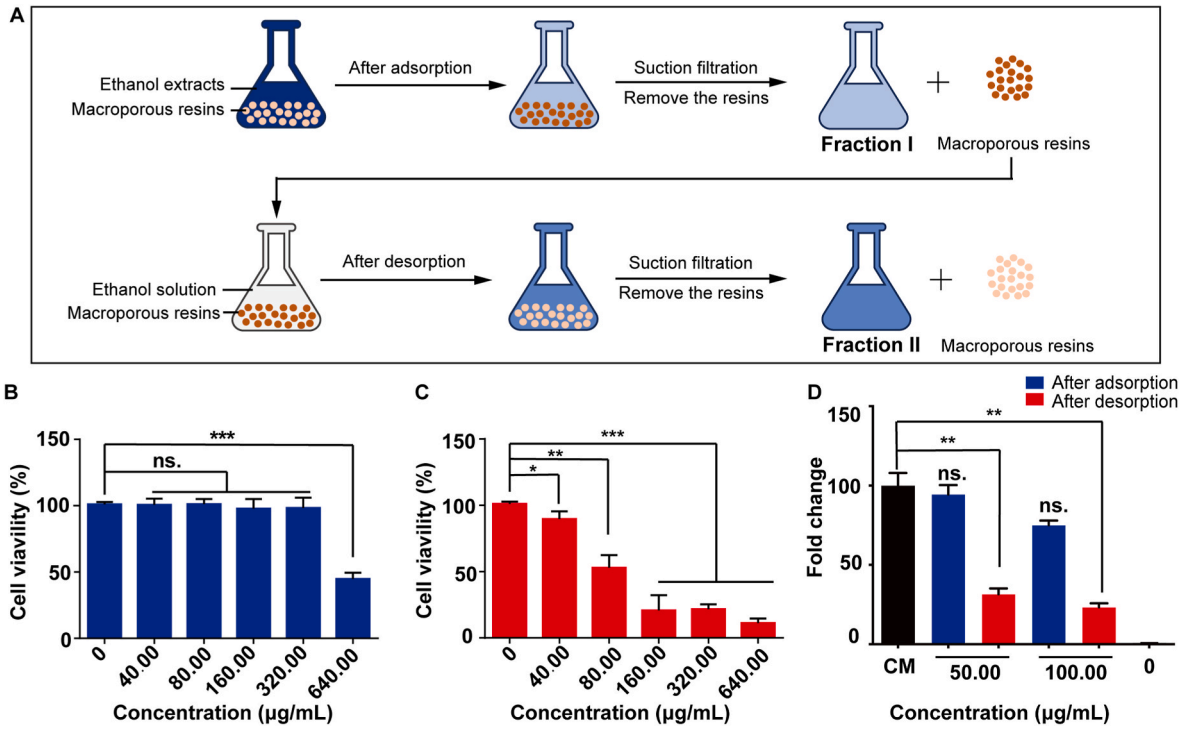

Fig. 2. The effects of different fractions on the viability of RKO cells and the Wnt signaling. A. The illustration of the experimental design workflow. B. MTT assay for the fraction after adsorption (fraction I) in RKO cells. C. MTT assay for the fraction after desorption (fraction II) in RKO cells. D. Dual-luciferase reporter assay for the fraction I and II. $*p < 0.05$, $**p < 0.01$, $***p < 0.001$. (Student's two tailed *t*-test).

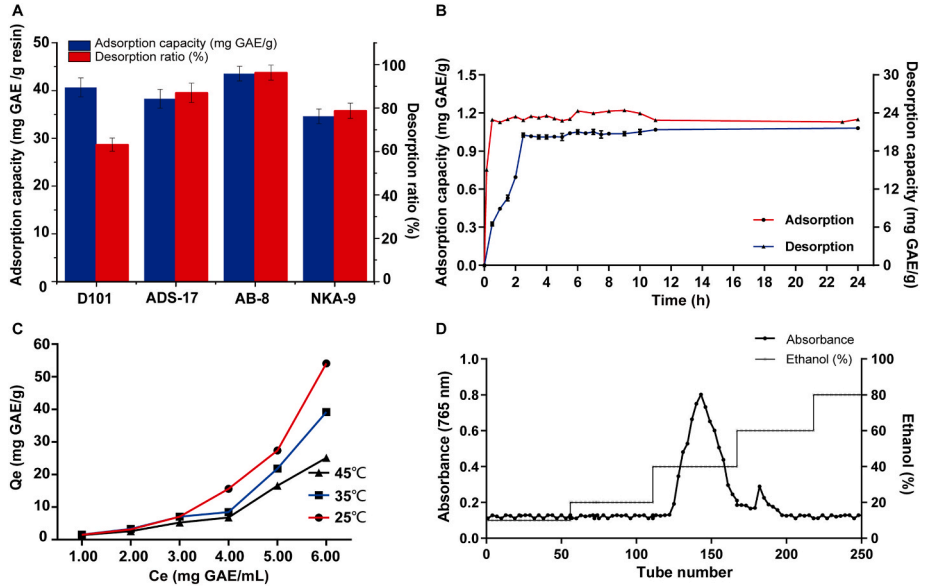

Fig. 3. Purification of polyphenols from *Citrus aurantium* L. with AB-8 macroporous resins. A. Adsorption and desorption properties of the D101, ADS-17, AB-8 and NKA-9 macroporous resins. B. Static adsorption and desorption kinetic curves of the Citrus aurantium L. polyphenols on AB-8 resins. C. Adsorption isotherm curves for Citrus aurantium L. polyphenols on AB-8 resins at different temperatures. D. Dynamic desorption curve of the ethanol extracts.

static adsorption and desorption method (Fig. 2A). The fraction after adsorption (fraction I) was obtained and most of its phenolic compounds were removed (TPC: 2.32 ± 1.13%). The fraction desorbed from the AB-8 resins (fraction II) was rich in phenolic compounds (23.18 ± 1.92%). The MTT analysis proved the obvious differences between fractions I and II. After fraction I was deprived of most of its phenolic compounds, it lost the ability to inhibit the growth of RKO cells (Fig. 2B). To the contrary, fraction II could significantly inhibit the viability of RKO cells even at the powder concentration of 40.00 μg/mL indicating that fraction II still retained the anti-CRCs activity (Fig. 2C). To further verify the involvement of the two fractions in the Wnt signaling inhibitory activity, dual-luciferase reporter system was employed. It turned out that fraction I was not able to attenuate the Wnt signaling, while fraction II dose-dependently attenuated Wnt signaling ($p < 0.01$) (Fig. 2D), which is consistent with the previous MTT results. These results suggested that phenolic compounds might be the main effective constituents in *Citrus*

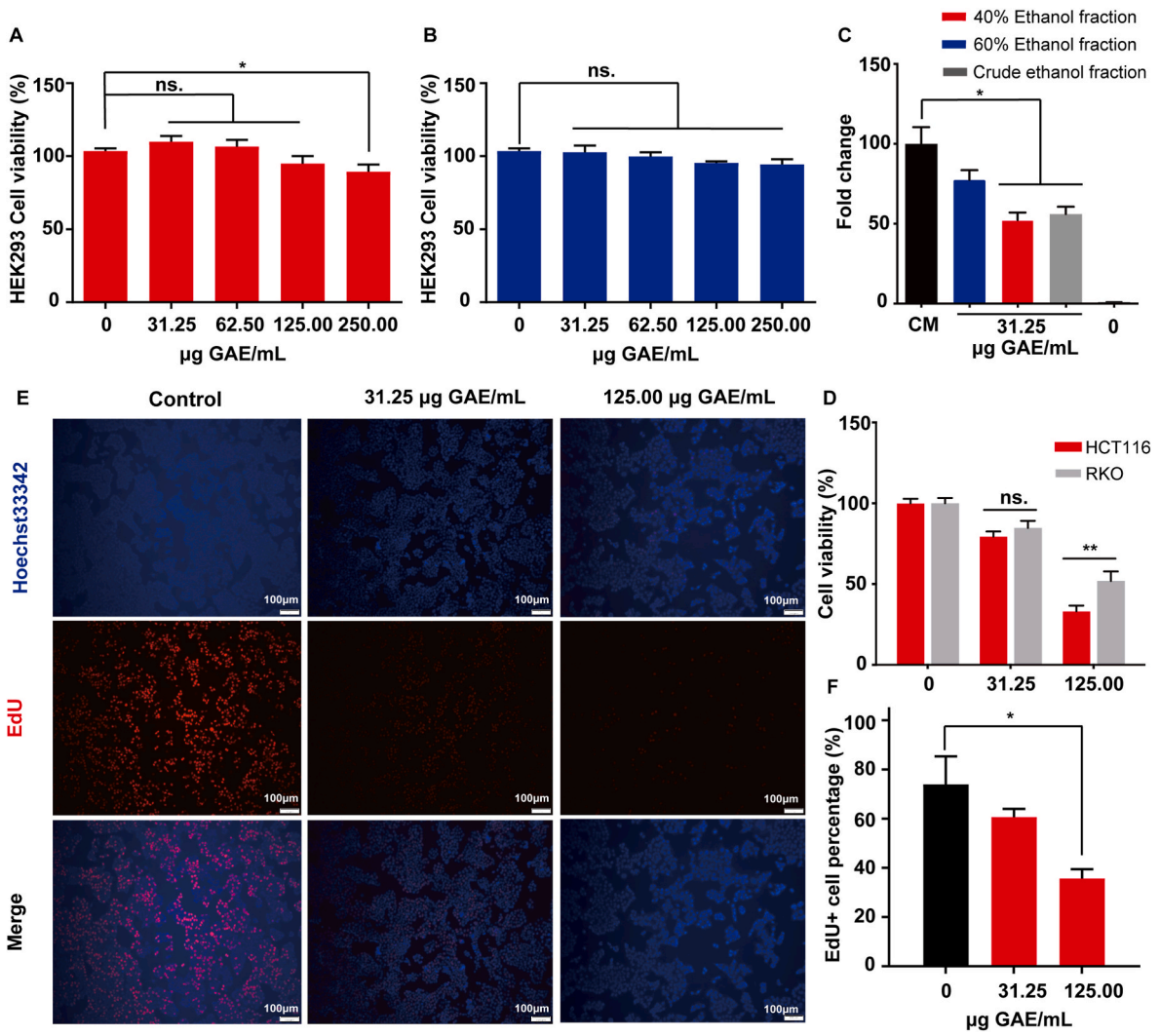

Fig. 4. The purified fraction showed anti-proliferative activity against Wnt-dependent HCT116 cells by attenuating the Wnt signaling. A. MTT assay for the 40% ethanol eluant in HEK293 cells. B. MTT assay for the 60% ethanol eluant in HEK293 cells. C. Dual-luciferase reporter assay for the 40% and 60% ethanol eluants. D. MTT assay for the 40% ethanol eluant in HCT116 and RKO cells. E. EdU assay for 40% ethanol eluants in HCT116 cells. F. Quantification of EdU + cells by image J software. $*p < 0.05$, $**p < 0.01$, $***p < 0.001$. (Student's two tailed *t*-test).

aurantium L. extracts accounting for the inhibition of RKO cells.

3.3. Purification of the Citrus aurantium L. polyphenols

Since phenolic compounds were confirmed as the effective constituents of the ethanol extract of *Citrus aurantium* L., obtaining phenolic rich fraction is necessary for further investigation on the mechanism of action. Enriching the polyphenol compounds by ethanol extraction alone is not sufficient. Therefore, further purification process is necessary to obtain phenolic fraction of high purity.

Firstly, the purification conditions were explored and optimized. Macroporous resins are commonly used for isolation of phenolic compounds due to their low-cost, eco-friendly nature and most importantly the potential for large-scale industrial production (Wang et al., 2020). Selection of the suitable macroporous resins was the first step to ensure that phenolic compounds could be effectively enriched. Static adsorption and desorption experiments showed that AB-8 resins have both the highest adsorption capacity (43.79 ± 1.92 mg GAE/g resin) and desorption ratio (92.69 ± 2.18%) (Fig. 3A), making it preferentially appropriate for *Citrus aurantium* L. polyphenols isolation. The adsorption and desorption kinetic curves based on AB-8 resins were presented in Fig. 3B. It takes around 2.5 h to reach adsorption equilibrium and only about 0.5 h to reach desorption equilibrium. The results were similar to the adsorption and desorption kinetics of AB-8 resins on *Ipomoea batatas* L. polyphenols (Xi et al., 2015). In addition, the adsorption isotherms of polyphenols on AB-8 resins at 25°C, 35°C, and 45°C were investigated (Fig. 3C). Lower temperature was ideal for the adsorption of polyphenols onto AB-8 resins as the highest adsorption capacity was reached at 25°C, which indicated the adsorption process was an exothermic reaction. Similar studies also reported that the adsorption of phenolic compounds was inversely proportional to temperature (Che Zain et al., 2020; Hou and Zhang, 2021). This may be because the polyphenol molecules acquire higher kinetic energies and resins swell as temperature increases (L. Sun et al., 2013). Additionally, the difference in adsorption capacity may probably be related to the properties of the macroporous resins and the characteristics of the phenolic compounds (Wang et al., 2020).

Consequently, AB-8 resins, 2.5 h static adsorption time and a temperature of 25°C were chosen as the optimal conditions for the next dynamic purification process. Varying concentrations of ethanol/water solvents (20%, 40%, 60%, 80% v/v) were then used for the dynamic adsorption and desorption. The dynamic desorption curves indicated that only two peak fractions were obtained; one each from the 40% and 60% ethanol eluants (Fig. 3D). These two purified fractions were then collected for subsequent bioactivity validation.

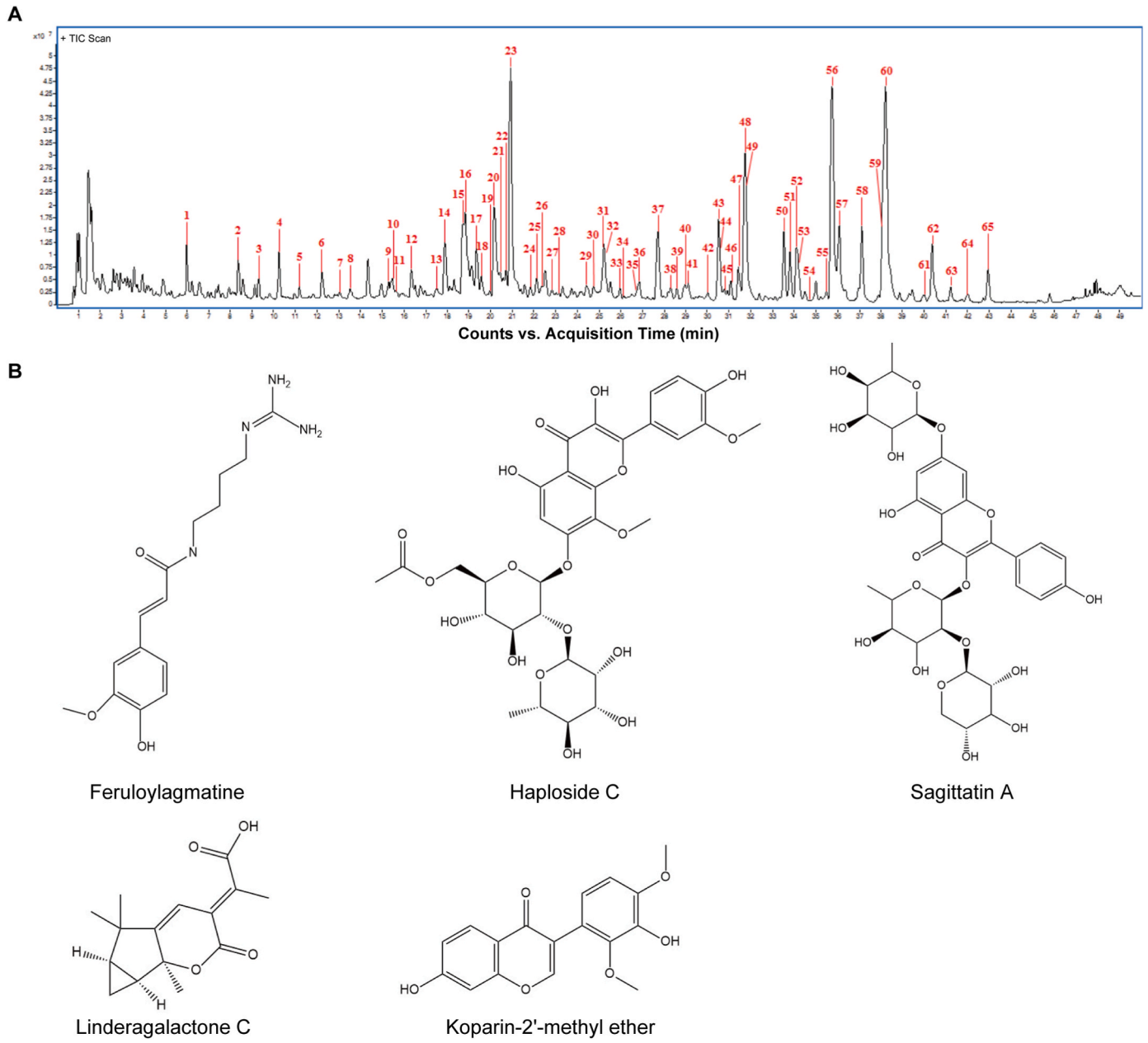

Fig. 5. Compound identification of 40% ethanol eluant by UHPLC-Q-TOF/MS. A. UHPLC-Q-TOF chromatogram for 40% ethanol eluant. B. Structure for Feruloylagmatine, Haploside C, Sagittatin A, Linderagalactone C and Koparin-2′-methyl ether.

3.4. Purified fraction of Citrus aurantium L. suppressed the proliferation of Wnt-dependent CRCs

To evaluate the cytotoxicity of the purified fraction, MTT assay was applied on normal cells. The 40% and 60% ethanol elution fractions both showed non-toxic effect on the viability of normal cells (HEK293 cells) below the concentration of 125.00 μg GAE/mL (Fig. 4A and B), indicating a maximum allowable concentration for further study. Subsequently, dual-luciferase reporter assay was used to examine the Wnt signaling inhibitory activity of both the 40% and 60% ethanol elution fractions. In addition, we found the 40% ethanol elution fraction to be a robust antagonist to the Wnt signaling pathway (Fig. 4C), inhibiting at similar levels to the crude ethanol extracts, suggesting the purification process still preserved the effective Wnt signaling inhibitory components. To evaluate if 40% ethanol elution fraction possesses selectivity on Wnt-dependent CRCs, HCT116 cells are used for verification. Differ from RKO cells, HCT116 cells are Wnt-dependent CRCs, persisting the whole Wnt signaling pathway and in a hyper-activation state (Fafilek et al., 2013). MTT results indicated that 40% ethanol elution fraction showed higher inhibitory effect on HCT 116 cells (33.24 ± 3.44%) than that of RKO cells (51.89 ± 5.91%) at 125.00 μg GAE/mL (Fig. 4D), which is consistent with the hypothesis. Besides, EdU assay was applied to further confirm its anti-proliferative activity on HCT116 cells (Fig. 4E). The 40% ethanol elution fraction triggered a dose-dependent inhibition of HCT116 cells and induced a reduction in proliferation rate to 57.18 ± 6.55% and 37.48 ± 6.84% at 31.25 and 125.00 μg GAE/mL, respectively (Fig. 4F). Taken together, these results suggest the possible mechanism by which the 40% ethanol elution fraction represses the proliferation of HCT116 cells may be attributable to the inhibition of the Wnt signaling.

However, our present work has limitations. Multiplexed cell-based assays are still needed to verify its mechanisms, such as the target validation of the Wnt signaling. Furthermore, *in vivo* experiments are necessary to study its behavior in the complex physiological context and

Table 1
Compounds identified in the 40% ethanol eluant from *Citrus aurantium* L. ethanol extracts by UHPLC-Q-TOF/MS.

No.	t_R (min)	[M+H]+ (m/z)	[M+Na]+ (m/z)	Compound formular	Diff (ppm)	Fragment ions (m/z)	Identification
1	5.96	205.0972		$C_{11}H_{12}N_2O_2$	−0.48	188, 170, 159, 146, 132, 118	Tryptophan (PubChem CID: 6305)
2	8.35	265.1547		$C_{14}H_{20}N_2O_3$	−0.39	248, 219, 177, 145, 117	Subaphyllin (PubChem CID: 5281796)
3	9.29	487.1451	509.1264	$C_{21}H_{26}O_{13}$	−1.07	179, 163, 129	Unknown 1
4	10.23	487.1453	509.1268	$C_{21}H_{26}O_{13}$	−1.57	221, 179, 129,	Unknown 2
5	11.16	307.1766		$C_{15}H_{22}N_4O_3$	−0.63	290, 265, 248, 177, 145, 131, 114	Feruloylagmatine (PubChem CID: 46173376)
6	12.2	595.1659	617.1459	$C_{27}H_{30}O_{15}$	−1.02	577, 559, 541, 523, 481, 457, 439, 421, 409, 403, 391, 379, 361, 355, 349, 337, 325, 307, 295, 283	Apigenin-6,8-di -C-glucoside (PubChem CID: 3084407)
7	13.01	625.1774	647.1589	$C_{28}H_{32}O_{16}$	−1.6	607, 589, 571, 553, 535, 511, 487, 469, 439, 409, 385, 367, 355, 337, 325	Diosmetin-6,8-di -C-glucoside
8	13.51	625.1769		$C_{28}H_{32}O_{16}$	−0.91	607, 589, 571, 553, 535, 511, 487, 469, 439, 409, 385, 367, 355, 337, 325, 313	Diosmetin 6,8-di -C-glucoside (isomer)
9	15.28	471.2021		$C_{26}H_{30}O_8$	−1.55	453, 425, 407, 367, 339, 161, 95	Limonin (PubChem CID: 179651)
10	15.46	597.1821		$C_{27}H_{32}O_{15}$	−1.11	415, 381, 355, 331, 289, 263, 245, 219, 195, 163,153, 129	Eriocitrin (PubChem CID: 83489)
11.	15.58	481.1682		$C_{23}H_{28}O_{11}$	5.00	415, 319, 301	Albiflorin (PubChem CID: 24868421)
12	16.32	597.1821		$C_{27}H_{32}O_{15}$	−1.31	485, 417, 381, 355, 331, 289, 263, 245, 219, 195, 163, 153, 129	Neoeriocitrin (PubChem CID: 114627)
13	17.49	595.1665		$C_{27}H_{30}O_{15}$	−1.08	449, 413, 379, 287, 271, 195	Veronicastroside (PubChem CID: 5282152)
14	17.89	581.187	603.168	$C_{27}H_{32}O_{14}$	−1.57	419, 401, 365, 339, 315, 297, 285, 273, 263, 245, 219, 195, 153, 129	Naringenin-7-O-rutinoside (Narirutin) (PubChem CID: 442431)
15	18.7	581.1869	603.1677	$C_{27}H_{32}O_{14}$	−0.92	417, 399, 383, 365, 351, 339, 315, 297, 285, 273, 263, 245, 219, 195, 153, 129	Naringenin-7-O-neohesperidoside (PubChem CID: 442428)
16	18.8	435.1291		$C_{21}H_{22}O_{10}$	−0.98	399, 381, 363, 351, 339, 297, 285, 273, 261, 231, 219, 195, 165, 153	Naringenin-7-O -glucoside (PubChem CID: 9910767)
17	19.33	611.1979	633.1792	$C_{28}H_{34}O_{15}$	−1.52	449, 431, 413, 395, 369, 345, 327, 315, 303, 297, 281, 263, 245, 219, 195, 177, 153, 129	Hesperetin-7-O-rutinoside (Hesperidin) (PubChem CID: 10621)
18	19.55	579.1708		$C_{27}H_{30}O_{14}$	−1.07	433, 381, 313, 271, 229, 195, 129	Apigenin-7-O-rutinoside (Isorhoifolin) (PubChem CID: 9851181)
19	19.94	609.1822		$C_{28}H_{32}O_{15}$	−1.24	463,431,413,395, 369, 345,327, 315,301,286, 263, 245, 219, 195, 177, 153, 129	Diosmetin-7-O-rutinoside (Diosmin) (PubChem CID: 5281613)
20	20.16	611.1979	633.1788	$C_{28}H_{34}O_{15}$		449, 431, 413, 395, 369, 345, 327, 315,303, 297, 281, 263, 245, 219, 195, 177, 153, 129	Hesperetin-7-O-Neohesperidoside (Neohesperidin) (PubChem CID: 442439)
21	20.42	465.1403		$C_{22}H_{24}O_{11}$	−2.33	369, 303, 285, 231, 219, 195, 177, 153	Hesperitin-7-O-glucoside (PubChem CID: 147394)
22	20.59	609.1819		$C_{28}H_{32}O_{15}$	−2.63	449, 429, 413, 395, 381, 369, 345, 327, 315, 301, 286, 263, 245, 219, 195, 177, 153, 129	Diosmetin-7-O-Neohesperidoside (Neodiosmin) (PubChem CID: 91746157)
23	20.9	261.1142		$C_{15}H_{18}O_5$	−1.74	243, 189, 159, 131	Meranzin hydrate (PubChem CID: 5070783)
24	21.8	277.1073	299.089	$C_{15}H_{16}O_4$	−0.93	259, 241, 217, 189, 131	Linderanlide A
25	22.09	667.1877	689.1687	$C_{30}H_{34}O_{17}$	−1.19	401, 383, 365, 339, 315, 297, 273, 263, 231, 195, 153, 127	Naringin-6''-malonate (PubChem CID: 101711437)
26	22.32	725.2301	747.2109	$C_{33}H_{40}O_{18}$	−1.6	491, 447, 381, 339, 315, 297, 273, 261, 219, 195, 153, 127	Unknown 3
27	22.82	625.2138	647.1947	$C_{29}H_{36}O_{15}$	−0.74	565, 409, 383, 359, 341, 329, 317, 281, 263, 245, 219, 195, 179, 153, 129	Magnoloside A (PubChem CID: 73189372)
28	23.14	697.1985	719.1786	$C_{31}H_{36}O_{18}$	−1.23	449, 431, 413, 391, 369, 345, 327, 303, 285, 263, 245, 219, 195, 177, 153, 127	Haploside C (PubChem CID: 44260015)
29	24.36	595.2033	617.284	$C_{28}H_{34}O_{14}$	−1.68	397, 379. 353, 287, 263, 219, 195, 153	Neoponcirin (PubChem CID: 85705)
30	24.74	291.1232		$C_{16}H_{18}O_5$	−1.4	273, 242, 219, 207, 189, 161	Linderanlide D
31	25.2	595.2028	617.1838	$C_{28}H_{34}O_{14}$	−1.42	397, 379. 353, 287, 263, 219, 195, 153	Poncirin (PubChem CID: 442456)
32	25.22	287.0914		$C_{16}H_{14}O_5$	−0.08	161, 153, 133	Oxypeucedanin (PubChem CID: 160544)
33	25.93	711.2135	733.1949	$C_{32}H_{38}O_{18}$	−0.71	405, 390, 375, 347, 187, 165, 145, 127	Sagittatin A or isomer (PubChem CID: 44258946)
34	26.11	697.1987	719.18	$C_{31}H_{36}O_{18}$	−1.4	391, 376, 361, 343, 187, 169, 145, 127	Haploside C isomer
35	26.71	697.1984	719.1788	$C_{31}H_{36}O_{18}$	−1.11	391, 376, 361, 343, 187, 169, 145, 127	Haploside C isomer
36	26.8	728.3983	750.3805	$C_{36}H_{53}N_7O_9$	−1.09	700, 615, 587, 502, 474, 405, 377, 339, 282, 242, 138	Citrusin III
37	27.72	273.076		$C_{15}H_{12}O_5$	−0.83	255, 231, 213, 189, 179, 153, 147,	Naringenin (PubChem CID: 932)
38	28.3	193.0494		$C_{10}H_8O_4$	−1.43	178, 165, 150, 137, 133	Scopoletin (PubChem CID: 5280460)

(*continued on next page*)

Table 1 (*continued*)

No.	t_R (min)	[M+H]+ (m/z)	[M+Na]+ (m/z)	Compound formular	Diff (ppm)	Fragment ions (m/z)	Identification
39	28.56	725.2301	747.2114	$C_{33}H_{40}O_{18}$	−1.99	461, 419, 404, 389, 371, 361, 328, 313, 271, 253, 187, 165, 145, 127	Melitidin (PubChem CID: 101485562)
40	28.91	329.1026		$C_{18}H_{16}O_6$	−1.58	314, 299, 285, 268, 239	Monohydroxytrimethoxyflavone
41	29.09	303.0867		$C_{16}H_{14}O_6$	−0.98	285, 261, 243, 219, 201, 177, 153, 145	Hesperetin (PubChem CID: 72281)
42	30	263.1281		$C_{15}H_{18}O_4$	−0.85	245, 230, 217, 203, 161	Linderagalactone C (PubChem CID: 102597495)
43	30.48	355.1523		$C_{21}H_{22}O_5$	4.72	337, 283, 262, 193, 185	Epoxybergamottin or Cnidicin (PubChem CID: 9946625 or 10043694)
44	30.5	704.3984	726.3802	$C_{34}H_{53}N_7O_9$	−1.3	573, 555, 502, 484, 419, 391, 318, 306, 288, 249, 221, 185, 157	Citrusin I (PubChem CID: 15232519)
45	30.75	389.1239		$C_{20}H_{20}O_8$	−1.82	374, 359, 341, 197, 163	Monohydroxy-Pentmethoxyflavone
46	31.06	359.113	381.0942	$C_{19}H_{18}O_7$	−1.39	359, 344, 329, 283, 211	5-Hydroxy-6,7,3′,4′-tetramethoxy flavone (PubChem CID: 5318355)
47	31.4	373.1289	395.1101	$C_{20}H_{20}O_7$	−1.88	358, 343, 329, 315, 273,	Isosinensetin (PubChem CID: 632135)
48	31.71	261.1137	283.0944	$C_{15}H_{16}O_4$	−1.6	243, 189, 159, 131	Meranzin or IsoMeranzin (PubChem CID: 1803558 or 3819217)
49	31.75	389.124	411.1042	$C_{20}H_{20}O_8$	−2.36	374, 359, 341, 183, 127	Monohydroxy-pentmethoxyflavone
50	33.51	373.129	395.1097	$C_{20}H_{20}O_7$	−1.95	358, 343, 329, 312	Sinensetin (PubChem CID: 145659)
51	33.79	343.1179		$C_{19}H_{18}O_6$	−0.76	328, 313, 299, 285, 267, 257	Tetramethyl-O-isoscutellarein (PubChem CID: 629964)
52	34.09	355.155		$C_{21}H_{22}O_5$	−2.59	257, 243, 215, 203, 187, 175, 153, 135	Epoxybergamottin or Cnidicin (PubChem CID: 9946625 or 10043694)
53	34.17	471.2021	493.183	$C_{26}H_{30}O_8$	−2.06	453, 425, 407, 367, 339, 161, 95	Limonin isomer
54	34.85	315.0866		$C_{17}H_{14}O_6$	−0.95	300, 283, 271, 254	Koparin-2′-methyl ether. (PubChem CID: 6710647)
55	35.44	345.0974	367.079	$C_{18}H_{16}O_7$	−1.64	330, 315, 297, 284, 256, 227, 197, 169,	Eupatorin (PubChem CID: 97214)
56	35.84	403.1394	425.1205	$C_{21}H_{22}O_8$	−1.44	388, 373, 355, 342, 301	Nobiletin (PubChem CID: 72344)
57	36.06	343.1187	365.0994	$C_{19}H_{18}O_6$	−2.77	328, 313, 299, 282, 253	Tetramethyl-O-scutellarein (5,7,8,4′-tetramethoxyflavone) (PubChem CID: 96118)
58	37.1	433.1503	455.1315	$C_{22}H_{24}O_9$	−1.9	418, 403, 385, 375, 357, 329, 211, 165	3,5,6,7,8,3′,4′-Heptamethoxyflavone (PubChem CID: 150893)
59	38.06	419.1348	441.1155	$C_{21}H_{22}O_9$	−0.79	404, 389, 371, 361, 343, 328, 315, 303, 211, 165	Monohydroxy-hexamethoxyflavone
60	38.19	373.1285	395.1099	$C_{20}H_{20}O_7$	−1.06	358, 343, 325, 312, 297	Tangeretin (PubChem CID: 68077)
61	39.96	403.1395	425.1206	$C_{21}H_{22}O_8$	−1.71	388, 373, 355, 345, 327, 315, 259, 227, 211, 183, 165, 145, 135	Hexamethoxyflavone (PubChem CID: 72344)
62	40.33	389.1239	411.1054	$C_{20}H_{20}O_8$	−0.54	374, 359, 341, 328, 313, 298, 197, 165	5′-hydroxy-3, 5, 6, 2′, 4′-pentamethoxyflavone (PubChem CID: 11079623)
63	41.2	389.1235	411.1052	$C_{20}H_{20}O_8$	−1.07	374, 359, 341, 331, 313, 298	Monohydroxy-pentmethoxyflavone
64	41.98	245.1176	267.099	$C_{15}H_{16}O_3$	−1.22	189, 159, 131, 103	Osthole (PubChem CID: 10228)
65	42.92	359.1129	381.0947	$C_{19}H_{18}O_7$	−1.11	359, 344, 329, 311, 298, 270, 255, 242, 227, 197, 169	7-hydroxy-5,6,8,4′-tetramethoxyflavone (PubChem CID: 5318356)

further evaluate its anti-CRC function. Nevertheless, this work provides the basis for potential candidates for functional food materials. The significance of our work for screening potential bioactive compounds from the complicated food materials in a time-efficient manner may be a stepping stone for further testing in *in vivo* animal studies.

The constituents of the 40% ethanol elution fraction were further analyzed using UHPLC-Q-TOF/MS. Chromatographic conditions were optimized allowing the successful separation of most chemical components using the positive ion mode. Fig. 5A showed the typical MS total ion current (TIC) chromatogram of 65 phytochemicals that were successfully characterized. A summary of the identified compounds with their retention times, MS/MS spectra and identifying ions are presented in Table 1. Some phytochemicals identified are reported to have potential anti-CRCs activity, such as limonin (Ishak et al., 2021), hesperetin-7-O-rutinoside (J. Sun et al., 2022), naringenin (Cheng et al., 2020), oxypeucedanin (Kim et al., 2007), scopoletin (Tabana et al., 2016), eupatorine (Sarvestani et al., 2015), nobiletin (Goh et al., 2019), tangeretin (Ting et al., 2015) and osthole (Yang et al., 2021). Notably, five of the phytochemicals were tentatively identified in *Citrus aurantium* L. for the first time (Fig. 5B). Feruloylagmatine has only been detected in several accessions (Gorzolka et al., 2014; Jin and Yoshida, 2000; Muroi et al., 2009; Yogendra et al., 2017) and Haploside C was found in both *Haplophyllum perforatum*. and *Haplophyllum foliosum*. (Batirov et al., 1987; Yuldashev, 2001), but yet to be reported in *Citrus aurantium* L. Sagittatin A was only previously detected in both *Randonia africana Coss.* and *Epimedium sagittatum* (Berrehal et al., 2010; Oshima et al., 1989). A similar situation was also observed for Linderagalactone C and Koparin-2′-methyl ether, which have only been identified in *Lindera aggregate* and *Teucrium polium* L, respectively (Alreshidi et al., 2020; Wu et al., 2010). This finding may provide new potential candidates for further functional ingredients evaluation for CRC management. Due to the difficulties in single compound purification, the anti-CRC roles of the five compounds in anti-CRC remain to be determined.

This study sheds more light on the active constituents of *Citrus aurantium* L. fruit and thus might stimulate a greater interest in exploring the possible application of these bioactive compounds in functional food ingredients.

4. Conclusion

A separation of phenolic rich fraction with anti-CRCs activity from *Citrus aurantium* L. by bioactivity guided rule was carried out in this work. In this bioactive phenolic rich fraction, the predominant components (65 compounds) were identified by UHPLC-Q-TOF/MS analysis. Notably, there were five phytochemicals (Feruloylagmatine, Haploside C, Sagittatin A, Linderagalactone C and Koparin-2′-methyl ether) identified in *Citrus aurantium* L. fruit for the first time. Taken together, this work showed that, simultaneously evaluating the activity of each

fraction during the whole process is critical to discriminate potential bioactive components and optimize the key technologies. It would be intriguing in the future to develop the *Citrus aurantium* L.-derived polyphenols as potential natural source of dietary agents in functional food industry for nutrition intervention in CRC.

CRediT authorship contribution statement

Li Gao: Investigation, Formal analysis, Writing – original draft, Writing – review & editing. **Na Gou:** Investigation, Methodology. **William Kwame Amakye:** Writing – review & editing. **Jianlin Wu:** Resources. **Jiaoyan Ren:** Resources, Supervision, Project administration.

Declaration of competing interest

The authors declare that they have no known competing financial interests or personal relationships that could have appeared to influence the work reported in this paper.

Acknowledgements

The authors gratefully acknowledge the Guangdong Province University Special Scientific Research Fund (2020KZDZX1017).

References

Almalki, W.H., 2021. Citrus aurantium flowers essential oil protects liver against ischemia/reperfusion injury. South Afr. J. Bot. 142, 325–334.
Alreshidi, M., Noumi, E., Bouslama, L., Ceylan, O., Veettil, V.N., Adnan, M., et al., 2020. Phytochemical screening, antibacterial, antifungal, antiviral, cytotoxic, and anti-quorum-sensing properties of Teucrium polium l. aerial parts methanolic extract. Plants 9 (11), 1418.
Batirov, E.K., Yuldashev, M., Khushbatkova, Z., Syrov, V., Malikov, V., 1987. Flavonoids ofHaplophyllum perforatum. Structure and hypoazotemic activity of haploside C. Chem. Nat. Compd. 23 (1), 54–57.
Berrehal, D., Khalfallah, A., Kabouche, A., Kabouche, Z., Karioti, A., Bilia, A., 2010. Flavonoid glycosides from Randonia africana Coss.(Resedaceae). Biochem. Systemat. Ecol. 38 (5), 1007–1009.
Che Zain, M.S., Lee, S.Y., Teo, C.Y., Shaari, K., 2020. Adsorption and desorption properties of total flavonoids from oil palm (Elaeis guineensis Jacq.) mature leaf on macroporous adsorption resins. Molecules 25 (4), 778.
Chen, L., Yu, B., Zhang, Y., Gao, X., Zhu, L., Ma, T., Yang, H., 2015. Bioactivity-guided fractionation of an antidiarrheal Chinese herb Rhodiola kirilowii (Regel) maxim reveals (-)-Epicatechin-3-Gallate and (-)-Epigallocatechin-3-Gallate as inhibitors of cystic fibrosis transmembrane conductance regulator. PLoS One 10 (3), e0119122.
Cheng, H., Jiang, X., Zhang, Q., Ma, J., Cheng, R., Yong, H., et al., 2020. Naringin inhibits colorectal cancer cell growth by repressing the PI3K/AKT/mTOR signaling pathway. Exp. Ther. Med. 19 (6), 3798–3804.
Degirmenci, H., Erkurt, H., 2020. Chemical profile and antioxidant potency of Citrus aurantium L. flower extracts with antibacterial effect against foodborne pathogens in rice pudding. LWT–Food Sci. Technol. 126, 109273.
Fafilek, B., Krausova, M., Vojtechova, M., Pospichalova, V., Tumova, L., Sloncova, E., et al., 2013. Troy, a tumor necrosis factor receptor family member, interacts with Lgr5 to inhibit Wnt signaling in intestinal stem cell. Gastroenterology 144 (2), 381–391.
Farahmandfar, R., Tirgarian, B., Dehghan, B., Nemati, A., 2020. Comparison of different drying methods on bitter orange (Citrus aurantium L.) peel waste: changes in physical (density and color) and essential oil (yield, composition, antioxidant and antibacterial) properties of powders. J. Food Meas. Char. 14 (2), 862–875.
Gao, L., Gou, N., Yao, M., Amakye, W.K., Ren, J., 2021. Food-derived natural compounds in the management of chronic diseases via Wnt signaling pathway. Crit. Rev. Food Sci. 1–31.
Goh, J.X.H., Tan, L.T.-H., Goh, J.K., Chan, K.G., Pusparajah, P., Lee, L.-H., Goh, B.-H., 2019. Nobiletin and derivatives: functional compounds from citrus fruit peel for colon cancer chemoprevention. Cancers 11 (6), 867.
Gorzolka, K., Bednarz, H., Niehaus, K., 2014. Detection and localization of novel hordatine-like compounds and glycosylated derivates of hordatines by imaging mass spectrometry of barley seeds. Planta 239 (6), 1321–1335.
Hou, M., Zhang, L., 2021. Adsorption/desorption characteristics and chromatographic purification of polyphenols from Vernonia patula (Dryand.) Merr. using macroporous adsorption resin. Ind. Crop. Prod. 170, 113729.
Ishak, N., Mohamed, S., Madzuki, I., Mustapha, N., Esa, N., 2021. Limonin modulated immune and inflammatory responses to suppress colorectal adenocarcinoma in mice model. Naunyn-Schmiedeberg's Arch. Pharmacol. 394, 1907–1915.
Jayaprakasha, G.K., Mandadi, K.K., Poulose, S.M., Jadegoud, Y., Gowda, G., Patil, B.S., 2008. Novel triterpenoid from Citrus aurantium L. possesses chemopreventive properties against human colon cancer cells. Bioorg. Med. Chem. 16 (11), 5939–5951.
Jin, S., Yoshida, M., 2000. Antifungal compound, feruloylagmatine, induced in winter wheat exposed to a low temperature. Biosci., Biotechnol., Biochem. 64 (8), 1614–1617.
Khan, M.K., Zill-E-Huma, Da Ngles, O., 2014. A comprehensive review on flavanones, the major citrus polyphenols. J. Food Compos. Anal. 33 (1), 85–104.
Kim, Y., Kim, Y., Ryu, S., 2007. Antiproliferative effect of furanocoumarins from the root of Angelica dahurica on cultured human tumor cell lines. Phytother Res. 21 (3), 288–290.
Li, F., Yan, H., Jiang, L., Zhao, J., Lei, X., Ming, J., 2022. Cherry polyphenol extract ameliorated dextran sodium sulfate-induced ulcerative colitis in mice by suppressing Wnt/β-catenin signaling pathway. Foods 11 (1), 49.
Majnooni, M.-B., Mansouri, K., Gholivand, M.-B., Mostafaie, A., Mohammadi-Motlagh, H.-R., Afnanzade, N.-S., et al., 2012. Chemical composition, cytotoxicity and antioxidant activities of the essential oil from the leaves of Citrus aurantium L. Afr. J. Biotechnol. 11 (2), 498–503.
Muroi, A., Ishihara, A., Tanaka, C., Ishizuka, A., Takabayashi, J., Miyoshi, H., Nishioka, T., 2009. Accumulation of hydroxycinnamic acid amides induced by pathogen infection and identification of agmatine coumaroyltransferase in Arabidopsis thaliana. Planta 230 (3), 517–527.
Niedzwiecki, A., Roomi, M.W., Kalinovsky, T., Rath, M., 2016. Anticancer efficacy of polyphenols and their combinations. Nutrients 8 (9), 552.
Nusse, R., Clevers, H., 2017. Wnt/β-Catenin signaling, disease, and emerging therapeutic modalities. Cell 169 (6), 985–999.
Odeh, F., Rahmo, A., Alnori, A.S., Chaty, M.E., 2021. The cytotoxic effect of essential oils Citrus aurantium peels on human colorectal carcinoma cell line (Lim1863). J. Microb. Biotech. Food 1 (6), 1476–1487.
Oshima, Y., Okamoto, M., Hikino, H., 1989. Sagittatins A and B, flavonoid glycosides of Epimedium sagittatum Herbs1. Planta Med. 55 (3), 309–311.
Patil, J.R., Jayaprakasha, G., Murthy, K.C., Tichy, S.E., Chetti, M.B., Patil, B.S., 2009. Apoptosis-mediated proliferation inhibition of human colon cancer cells by volatile principles of Citrus aurantifolia. Food Chem. 114 (4), 1351–1358.
Pezzuto, J.M., 1997. Plant-derived anticancer agents. Biochem. Pharmacol. 53 (2), 121–133.
Ren, J., Zheng, Y., Lin, Z., Han, X., Liao, W., 2017. Macroporous resin purification and characterization of flavonoids from Platycladus orientalis (L.) Franco and their effects on macrophage inflammatory response. Food Funct. 8 (1), 86–95.
Sarikurkcu, C., Ozer, M.S., Tlili, N., 2019. LC-ESI-MS/MS characterization of phytochemical and enzyme inhibitory effects of different solvent extract of Symphytum anatolicum. Ind. Crop. Prod. 140, 111666.
Sarvestani, N., Sepehri, H., Farimani, M., 2015. Anticancer effect of eupatorin via bax/bcl-2 and mitochondrial membrane potential changes through ros mediated pathway in human colon cancer. Int. J. Pharmacogn. Phytochem. Res 7, 1039–1046.
Shehata, M.G., Awad, T.S., Asker, D., El Sohaimy, S.A., Abd El-Aziz, N.M., Youssef, M.M., 2021. Antioxidant and antimicrobial activities and UPLC-ESI-MS/MS polyphenolic profile of sweet orange peel extracts. Curr. Res. Food Sci. 4, 326–335.
Singh, B., Singh, J.P., Kaur, A., Singh, N., 2020. Phenolic composition, antioxidant potential and health benefits of citrus peel. Food Res. Int. 132, 109114.
Song, L., Li, Y., He, B., Gong, Y., 2015. Development of small molecules targeting the Wnt signaling pathway in cancer stem cells for the treatment of colorectal cancer. Clin. Colorectal Cancer 14 (3), 133–145.
Sun, C., Wu, Z., Wang, Z., Zhang, H., 2015. Effect of Ethanol/water Solvents on Phenolic Profiles and Antioxidant Properties of Beijing Propolis Extracts. Evid-Based Compl Alt, 2015.
Sun, J., Li, M., Lin, T., Wang, D., Chen, J., Zhang, Y., et al., 2022. Cell cycle arrest is an important mechanism of action of compound Kushen injection in the prevention of colorectal cancer. Sci. Rep. 12 (1), 1–16.
Sun, L., Guo, Y., Fu, C., Li, J., Li, Z., 2013. Simultaneous separation and purification of total polyphenols, chlorogenic acid and phlorizin from thinned young apples. Food Chem. 136 (2), 1022–1029.
Tabana, Y.M., Hassan, L.E.A., Ahamed, M.B.K., Dahham, S.S., Iqbal, M.A., Saeed, M.A., et al., 2016. Scopoletin, an active principle of tree tobacco (Nicotiana glauca) inhibits human tumor vascularization in xenograft models and modulates ERK1, VEGF-A, and FGF-2 in computer model. Microvasc. Res. 107, 17–33.
Ting, Y., Chiou, Y.-S., Pan, M.-H., Ho, C.-T., Huang, Q., 2015. In vitro and in vivo anti-cancer activity of tangeretin against colorectal cancer was enhanced by emulsion-based delivery system. J. Funct.Foods 15, 264–273.
Wang, Z., Peng, S., Peng, M., She, Z., Yang, Q., Huang, T., 2020. Adsorption and desorption characteristics of polyphenols from Eucommia ulmoides Oliv. leaves with macroporous resin and its inhibitory effect on α-amylase and α-glucosidase. Ann. Transl. Med. 8 (16), 1004.
Wu, Y., Zheng, Y., Liu, X., Han, Z., Ren, Y., Gan, L., et al., 2010. Separation and quantitative determination of sesquiterpene lactones in Lindera aggregata (Wu-yao) by ultra-performance LC-MS/MS. J. Separ. Sci. 33 (8), 1072–1078.
Xi, L., Mu, T., Sun, H., 2015. Preparative purification of polyphenols from sweet potato (Ipomoea batatas L.) leaves by AB-8 macroporous resins. Food Chem. 172, 166–174.
Yang, C., Song, J., Hwang, S., Choi, J., Song, G., Lim, W., 2021. Apigenin enhances apoptosis induction by 5-fluorouracil through regulation of thymidylate synthase in colorectal cancer cells. Redox Biol. 47, 102144.
Yogendra, K.N., Sarkar, K., Kage, U., Kushalappa, A.C., 2017. Potato NAC43 and MYB8 mediated transcriptional regulation of secondary cell wall biosynthesis to contain Phytophthora infestans infection. Plant Mol. Biol. Rep. 35 (5), 519–533.
Yuldashev, M., 2001. Flavonoids of Haplophyllum foliosum and H. pedicellatum. Chem. Nat. Compd. 37 (3), 288–289.